Draft version April 18, 2013
Preprint typeset using LaTeX style emulateapj v. 5/2/11

TIME-RESOLVED ANALYSIS OF FERMI GRBS WITH FAST AND SLOW-COOLED SYNCHROTRON PHOTON MODELS

J. M. Burgess[1,2], R. D. Preece[1,3], V. Connaughton,[1], M. S. Briggs[1], A. Goldstein[1], P. N. Bhat[1], J. Greiner[4], D. Gruber[4], A. Kienlin[4], C. Kouveliotou[5], S. McGlynn[6], C. A. Meegan[7], W. S. Paciesas[1], A. Rau[4], S. Xiong[1] and M. Axelsson[8,9,10], M. G. Baring[11,12], C. D. Dermer[13], S. Iyyani[9,14], D. Kocevski[15], N. Omodei[15], F. Ryde[10,9], G. Vianello[15,16]

Draft version April 18, 2013

ABSTRACT

Time-resolved spectroscopy is performed on eight bright, long gamma-ray bursts (GRBs) dominated by single emission pulses that were observed with the *Fermi Gamma-ray Space Telescope*. Fitting the prompt radiation of GRBs by empirical spectral forms such as the Band function leads to ambiguous conclusions about the physical model for the prompt radiation. Moreover, the Band function is often inadequate to fit the data. The GRB spectrum is therefore modeled with two emission components consisting of optically thin nonthermal synchrotron radiation from relativistic electrons and, when significant, thermal emission from a jet photosphere, which is represented by a blackbody spectrum. To produce an acceptable fit, the addition of a blackbody component is required in 5 out of the 8 cases. We also find that the low-energy spectral index α is consistent with a synchrotron component with $\alpha = -0.81 \pm 0.1$. This value lies between the limiting values of $\alpha = -2/3$ and $\alpha = -3/2$ for electrons in the slow and fast-cooling regimes, respectively, suggesting ongoing acceleration at the emission site. The blackbody component can be more significant when using a physical synchrotron model instead of the Band function, illustrating that the Band function does not serve as a good proxy for a nonthermal synchrotron emission component. The temperature and characteristic emission-region size of the blackbody component are found to, respectively, decrease and increase as power laws with time during the prompt phase. In addition, we find that the blackbody and nonthermal components have separate temporal behaviors.

Subject headings: acceleration of particles — gamma-ray bursts — gamma rays: stars — methods: data analysis — radiation mechanisms: non-thermal — radiation mechanisms: thermal

1. INTRODUCTION

The fireball model of GRBs (Cavallo & Rees 1978; Goodman 1986; Paczyński 1986) assumes that a large amount of energy is released in a small space leading to a fireball that emits γ-rays. The progenitors of these events are not known, but are believed to be the collapse of massive stars, or the coalescing of two compact objects. Details of this model rely heavily on assumptions about the initial parameters of the fireball including the radii of emission, the baryon load and the magnetic field associated with the plasma outflow (Mészáros 2006, for review see). The observed spectra of GRBs are typically interpreted as non-thermal (Piran 1999; Zhang et al. 2012) though there are some exceptions (Ryde 2004). This interpretation indicates that a dissipative process such as internal shocks energizes the electrons to non-thermal distributions. Though some versions of the fireball model predict that the entire spectrum in the γ-ray band be in the form of thermal emission, we concentrate on the version presented in Mészáros & Rees (2000) where a mixture of thermal and non-thermal (synchrotron) emission emerges. Alternative models such as the Poynting-flux dominated outflow (PFD) model exist and could provide a viable mechanism for generating the observed prompt emission. These PFD models have not yet advanced to quantitative spectral and temporal predictions; therefore, it is difficult to compare our results to theses models as extensively as is possible for the internal shock model for which extensive simulations of lightcurves and spectra have been developed (Daigne & Mochkovitch 1998; Bošnjak, Daigne, & Dubus 2009).

The physical emission process behind these extreme cosmic explosions has not been established. Histori-

james.m.burgess@nasa.gov
[1] University of Alabama in Huntsville, 320 Sparkman Drive, Huntsville, AL 35899, USA
[2] email: james.m.burgess@nasa.gov
[3] email: Rob.Preece@nasa.gov
[4] Max-Planck-Institut für extraterrestrische Physik (Giessenbachstrasse 1, 85748 Garching, Germany)
[5] Space Science Office, VP62, NASA/Marshall Space Flight Center, Huntsville, AL 35812, USA
[6] Exzellence Cluster "Universe", Technische Universitt Mnchen, Boltzmannstrasse 2, 85748, Garching, Germany
[7] Universities Space Research Association, 320 Sparkman Drive, Huntsville, AL 35899, USA
[8] Department of Astronomy, Stockholm University, SE-106 91 Stockholm, Sweden
[9] The Oskar Klein Centre for Cosmoparticle Physics, AlbaNova, SE-106 91 Stockholm, Sweden
[10] Department of Physics, Royal Institute of Technology (KTH), AlbaNova, SE-106 91 Stockholm, Sweden
[11] Rice University, Department of Physics and Astronomy, MS-108, P. O. Box 1892, Houston, TX 77251, USA
[12] email: baring@rice.edu
[13] Space Science Division, Naval Research Laboratory, Washington, DC 20375-5352, USA
[14] email: shabuiyyani@gmail.com
[15] W. W. Hansen Experimental Physics Laboratory, Kavli Institute for Particle Astrophysics and Cosmology, Department of Physics and SLAC National Accelerator Laboratory, Stanford University, Stanford, CA 94305, USA
[16] Consorzio Interuniversitario per la Fisica Spaziale (CIFS), I-10133 Torino, Italy

cally, GRB spectra have been best fit by a parametrized smoothly broken power-law that is connected exponentially, known as the Band function (Band et al. 1993)

$$F_\nu(\mathcal{E}) \;=\; F_0 \begin{cases} \left(\frac{\mathcal{E}}{100\ \mathrm{keV}}\right)^{\alpha} \exp\left(-\frac{(2+\alpha)\mathcal{E}}{E_{\mathrm{peak}}}\right) & \mathcal{E} \leq (\alpha-\beta)\frac{E_{\mathrm{peak}}}{(\alpha+2)} \\ \left(\frac{\mathcal{E}}{100\ \mathrm{keV}}\right)^{\beta} \exp(\beta-\alpha)\left[\frac{(\alpha-\beta)E_{\mathrm{peak}}}{100\ \mathrm{keV}(2+\alpha)}\right]^{\alpha-\beta} & \mathcal{E} > (\alpha-\beta)\frac{E_{\mathrm{peak}}}{(\alpha+2)} \end{cases} \quad (1)$$

where $\mathcal{E}$ is the photon energy. The Band function is characterized by its low and high-energy power-law indices (Band α and β respectively) as well as its νF_ν peak energy, E_{peak}. The ability of the Band function to fit most prompt-spectra has led to the ubiquitous use of the Band function's fitted parameters as indicators of the underlying emission and acceleration processes. In particular, the value of the low-energy index, Band α, has been of interest because non-thermal spectra differ most noticeably below their respective νF_ν peaks where the spectral index is fixed based on the type of emission (synchrotron, inverse-Compton, etc). Above the peak, the high-energy index is variable and related to the distribution of the emitting electrons and provides no clues for discerning between emission processes. Although such extrapolations can be useful, Burgess et al. (2011) (hereafter B11) directly fit a synchrotron photon model to the prompt emission data of GRB 090820A, showing that it is possible to fit a physical model directly to the data without relying on interpretations of the Band function in order to determine the process of γ-ray emission.

Previous studies (González et al. 2003; Guiriec et al. 2010; Guiriec et al. 2012; Ryde et al. 2010; Ryde 2005) showed that a single Band function cannot fully account for the spectrum of all GRBs. The addition of a blackbody and/or power-law better describes the spectra of these GRBs. Specifically, the addition of the blackbody below E_{peak} also allows for the direct fitting of the synchrotron model to the data, which we exploit in this work. The addition of a blackbody in the spectrum allows a quantitative analysis of its properties to ascertain its origin. Several studies (Mészáros & Rees 2000; Daigne & Mochkovitch 2002; Ryde 2004; Ryde et al. 2008) have developed the theoretical framework for a blackbody component coexisting with a non-thermal component in the spectra of GRBs, as well as testable relations that can be applied to data to investigate the photosphere of GRBs.

Herein, we extend the analysis of B11 to several bright *Fermi* GRBs and in addition we investigate the ability of the Band function to serve as a proxy for physical emissivities in the fitting process. We will show that slow-cooled synchrotron is a viable model for GRB prompt emission using data from both the Gamma-ray Burst Monitor (GBM) (10 keV to 40 MeV) and Large Area Telescope (LAT) (100 MeV - 300 GeV) on board the *Fermi* space telescope. This analysis makes use of the newly released LAT low-energy (LLE) data which provides a larger effective between 30 MeV and ∼1 GeV allowing us to extend the LAT analysis down to 30 MeV. First, we give a description of the non-thermal and blackbody photon emissivities (Section 2). We then present our analysis technique and compare the results with predictions about each component (Sections 3 and 4).

2. MODEL SPECTRAL COMPONENTS

In the fireball model of GRBs, the majority of the flux is theoretically expected to be in the form of thermal emission coming from the photosphere of the jet. However, over 2/3 of the low-energy indices recovered by the Band function are too soft to be thermal (Goldstein et al. 2012a,b). This points to a non-thermal emission process for most GRBs. Multi-spectral component analysis of *Fermi* GRBs has shown that while the majority of the emission is non-thermal, a small fraction of the energy radiated apparently originates from a blackbody component (Guiriec et al. 2011; Axelsson et al. 2012). In B11, a blackbody component was also identified when the non-thermal emission was fit with a synchrotron photon model. This combination of blackbody and non-thermal emission was predicted by Mészáros & Rees (2000). We further improve the analysis of B11 by first reviewing the synchrotron emission from cooled electrons and the slow-cooled synchrotron model from B11. In addition, we review several observable relations of the blackbody component. These components are then implemented into a fitting program which directly convolves the physical models with the GBM detector response to compare against the observations.

2.1. *Synchrotron Radiation*

While no definitive model for the non-thermal emission of GRBs exists, synchrotron is the simplest and most efficient non-thermal emission process that could account for the observed GRB radiation. It is a natural choice in the evolution from empirical fitting functions to physical models. In B11, we implemented a parametrized synchrotron model for fitting GRB data directly. We implemented a synchrotron model first used in fitting the deconvolved spectra of GRBs by Tavani (1996) and then later by Baring & Braby (2004). Sari, Piran, & Narayan (1998) identified two regimes for the synchrotron emission which are relevant for GRBs: fast and slow-cooling. The difference between the two is related to the radiative time-scale of the emission.

For the slow-cooling synchrotron model, we assume the electron distribution from B11 (see also Baring & Braby (2004)) which includes electrons in a thermal pool as well as electrons that are accelerated into a power-law tail (see Figure 1).

$$n_e(\gamma) \;=\; n_0\left[\left(\frac{\gamma}{\gamma_{\mathrm{th}}}\right)^2 e^{-\gamma/\gamma_{\mathrm{th}}} + \epsilon\left(\frac{\gamma}{\gamma_{\mathrm{th}}}\right)^{-\delta}\Theta\left(\frac{\gamma}{\gamma_{\min}}\right)\right], \quad (2)$$

Here, n_0 is the normalization, γ is the electron Lorentz factor, $\gamma_{\rm th}$ is the thermal electron Lorentz factor, $\gamma_{\rm min}$ is the minimum electron Lorentz factor of the power-law tail, ϵ is the normalization of the power-law, δ is the electron spectral index. The function $\Theta(x)$ is a step function where $\Theta(x) = 0$ for $x < 1$ and $\Theta(x) = 1$ for $x > 1$. There is strong evidence that sub-relativistic shock acceleration produces similar electron distributions to eq. 2 (Baring, Ellison, & Jones 1995). Recent developments in relativistic shock acceleration have shown that it is possible to accelerate electrons from a thermal pool into a power-law distribution (Spitkovsky 2008; Baring 2011; Summerlin & Baring 2012). These results motivate our choice of electron distribution even though our parametrization may oversimplify the process of acceleration and ignores the effects of photon-electron collisions such as Compton scattering that are likely taking place in the high γ-ray regime. Yet, the distribution we chose closely resembles the expected distribution resulting from shock acceleration in the absence of synchrotron cooling. The inclusion of the thermal electron component is physically required and is much closer to reality than the simple power-law electron distribution commonly invoked in GRB modeling. Simulations that include the full radiative heating and cooling of electrons expected in the high γ-ray regime but that neglect acceleration processes produce electron distributions that differ greatly from simple power-laws (Pe'er & Waxman 2004). These complicated electron distributions are difficult to model in a fitting process and may require spectral resolution beyond what the *Fermi* data provide to identify in spectral fits.

We convolve this simplified distribution with the standard isotropic synchrotron kernel (Rybicki & Lightman 1979)

$$F_\nu(\mathcal{E}) \;\propto\; \int_1^\infty n_e(\gamma)\,\mathcal{F}\left(\frac{\mathcal{E}}{\mathcal{E}_c}\right)\,d\gamma \quad , \tag{3}$$

where

$$\mathcal{F}(w) \;=\; w\int_w^\infty K_{5/3}(x)\,dx \tag{4}$$

expresses the single-particle synchrotron emissivity (i.e., energy per unit time per unit volume) in dimensionless functional form. The $K_{5/3}$ term is the modified spherical Bessel function. The characteristic scale for the synchrotron photon energy is

$$\mathcal{E}_c \;=\; E_*\gamma^2 \;, \tag{5}$$

where $E_* \equiv \frac{3}{2}\frac{\Gamma B}{B_{cr}}m_e c^2$, B is the global magnetic field strength, Γ is the bulk Lorentz factor, and $B_{\rm cr} = 4.41 \times 10^{13}$ Gauss is the quantum critical field.

In principle, there are six spectral parameters that can be constrained by the fits: n_0, E_*, δ, ϵ, $\gamma_{\rm th}$, and $\gamma_{\rm min}$; however, we fix $\gamma_{\rm th}$, $\gamma_{\rm min}$, and ϵ due to fitting correlations as explained below. The parameter E_* scales the energy of the fit and is linearly related to the Band function's $E_{\rm peak}$. Numerical simulations of GRB shocks have shown that the ratio of $\gamma_{\rm th}$ and $\gamma_{\rm min}$ is $\sim$3 (Baring & Braby 2004) and therefore we fix those parameters to have that ratio. The parameters E_*, $\gamma_{\rm th}$, and $\gamma_{\rm min}$ all directly scale the peak energy of the spectrum but do not alter its shape and thus cannot be independently determined. For this reason we chose values of $\gamma_{\rm th} = 10$ and $\gamma_{\rm min} = 30$ for all fits and left E_* free. Estimates of B, the magnetic field, and Γ are also not obtainable from these spectral fits because of the correlation between E_* and the electron Lorentz factors. For this reason the values of E_* from our fits are useful only for examining the evolution of the peak energy and not for obtaining the magnitude of B and Γ. It was found in B11 that the parameter ϵ, corresponding to the relative amplitude between the thermal and non-thermal portions of the electron distribution, was not easily constrained in the fitting process and produced non-physical electron distributions as pointed out in Beloborodov (2012). Therefore, we numerically fix this parameter so that there is no discontinuity between the thermal and non-thermal parts of the distribution. After these simplifications, three shape parameters remain free: E_*, δ and n_0, which corresponds to the amplitude. Compared with the Band function's four fit parameters this model is simpler yet tied to actual physical processes.

The second regime of synchrotron emission we examine is the so-called fast-cooling regime. Synchrotron is a very efficient process and cools electrons rapidly. In fact, the dynamic timescales associated with GRBs are much longer than the cooling timescales of synchrotron emission (Sari, Piran, & Narayan 1998). It is therefore necessary to investigate synchrotron emission from electrons that have been rapidly cooled. We assume that some acceleration process injects a power-law distribution of electrons

$$Q_e(\gamma) \;=\; q_e(\delta-1)\gamma_{\rm min}^{(\delta-1)}\gamma^{-\delta} \;,\; \gamma_{\rm min} \leq \gamma \tag{6}$$

into a region where they are allowed to cool. Here, q_e is the electron density. We neglect the inclusion of the thermal pool because its association with the radiative region is poorly understood. Moreover, we will show that the fast-cooling spectrum is already too broad for the typical GRB νF_ν peak and the thermal distribution only broadens the spectrum further. The cooling of electrons is governed by the continuity equation (Blumenthal & Gould 1970)

$$\frac{\partial n_e(\gamma,t)}{\partial t} + \frac{\partial}{\partial\gamma}[\dot{\gamma}n_e(\gamma,t)] + \frac{n_e(\gamma,t)}{t_{esc}} \;=\; Q_e(\gamma) \tag{7}$$

where n_e/t_{esc} represents the loss of particles from the emission region from which we can define the maximal cooling scale $\gamma/\dot{\gamma} \sim t_{esc}$. This corresponds to a Lorentz factor, γ_{cool}, below which cooling shuts off. We expect that γ_{cool} lies well below $\gamma_{\rm min}$ owing to the fact that a cooling break has not been observed in GRB data (however, see Ackermann et al. (2012b)). For very high electron Lorentz factors, $\gamma/\dot{\gamma} \ll t_{esc}$ and therefore the loss term can be neglected, i.e., the dynamical timescale is much longer than the radiative timescale. With this assumption we can simplify eq. 7 and it becomes time independent. The resulting electron distribution can then easily be solved for

$$n_e(\gamma,t) \;\approx\; \frac{1}{\dot{\gamma}}\int_\gamma^\infty Q_e(\gamma')d\gamma'. \tag{8}$$

Substituting in the synchrotron cooling rate

$$\dot{\gamma} = -\frac{\pi}{3}\frac{r_0 c}{r_g^2}\gamma^2 \tag{9}$$

where $r_g = m_e c^2/(eB)$ and $r_0 = e^2/(m_e c^3)$, eq. 8 yields the synchrotron-cooled broken power-law distribution of electrons (see Figure 2)

$$n_e^{cool} \propto \frac{q_e \gamma_{\min}}{\gamma^2} \min\left\{\left(\frac{\gamma}{\gamma_{\min}}\right)^{-(\delta-1)}, 1\right\}, \gamma_{cool} \leq \gamma. \tag{10}$$

This distribution is convolved with eq. 4 to produce a photon spectrum. The radiation spectrum generated by this distribution has an asymptotic low-energy index of $-3/2$, the so-called 'second line-of-death' (Cohen et al. 1997). The free parameters used for fitting this spectrum are the electron spectral index, δ, the fast-cooling equivalent of E_* and the overall amplitude. However, the majority of GRB spectra in the BATSE (Goldstein et al. 2012b) and GBM (Goldstein et al. 2012a) spectral catalogs have spectra with low-energy indices harder than $-3/2$. Even if the spectra were consistent with the low-energy index, the fast-cooling spectrum's curvature around the νF_ν peak is much broader than the peak of the data (See 4.2).

Such simplified models cannot capture all the nuances of a detailed simulation of the acceleration and radiation processes in GRBs. Both the cooled and uncooled models neglect self-absorption and Klein-Nishina effects which may be significant but which are beyond the scope of this investigation. One possible alternative to fitting parameterizied models is forming templates of spectra generated by a simulation and fitting those to data. The models implemented here already have degeneracies that require the fixing of certain parameters due to the lack of spectral resolution in the data. Simulations typically have more parameters than our current model (Pe'er & Waxman 2004; Asano, Inoue, & Mészáros 2009; Bošnjak, Daigne, & Dubus 2009) and constraining those models via spectral templates using data from *Fermi* will be difficult.

2.2. *Blackbody Component*

The pure fireball scenario for GRB emission predicts that most of the flux is from thermal emission (Goodman 1986; Paczyński 1986). This is because as the jet becomes optically thin at some photospheric radius, r_{ph}, it releases radiation that has undergone many scatterings with the optically thick electrons below the photosphere. We model this emission as a blackbody

$$F_\nu(\mathcal{E}) = A\mathcal{E}^3 \frac{1}{e^{\frac{\mathcal{E}}{kT}} - 1} \tag{11}$$

where A is the normalization and kT scales the energy of the function. This is simplified thermal emission from the photosphere that does not take into account the effects of relativistic broadening that can produce a multi-color blackbody emerging from the photosphere (Beloborodov 2010; Ryde et al. 2010; Pe'er & Ryde 2011). Ryde et al. (2008) showed that if it is assumed that the thermal component is emanating from the photospheric radius of the jet, several properties about the blackbody component are derivable. In particular, the ratio of the thermal (U_{BB}) and non-thermal (U_{non-th}) flux is given by

$$\frac{U_{BB}}{U_{non-th}} \propto \frac{\sigma_{sb} T^4}{\rho} \propto T \tag{12}$$

where ρ is the density of the plasma, σ_{sb} is the Stefan-Boltzmann constant, and $kT \propto \rho^{1/3}$. The cooling behavior is also well predicted for a thermal component. The temperature should decay as $T \propto t^{-2/3}$. It has been found that the evolution of kT often follows a broken power-law trend with the index below the break averaging to $\sim -2/3$ (Ryde and Pe'er 2009). Finally, a true blackbody has a well defined relation between energy flux and temperature:

$$F_{BB} = N\sigma_{sb} T^4 \tag{13}$$

where N is a normalization accounting for geometrical effects.

The photospheric radius and the transverse size of the photospheric emitting region are also of great importance to understanding the geometry and energetics of GRBs. In Ryde and Pe'er (2009), a parameter $\mathcal{R}$

$$\mathcal{R}(t) \equiv \left(\frac{F_{BB}(t)}{\sigma_{sb} T(t)^4}\right)^{1/2} \propto r_{ph}. \tag{14}$$

is used to track the outflow dynamics of the burst. Several BATSE GRBs were found to have a power-law increase of $\mathcal{R}$ with time. However, the connection between $\mathcal{R}$, T, and F_{BB} was difficult to establish because the error on the data points was large. Understanding these connections is essential to unmasking the structure and temporal evolution of GRB jets.

3. TIME RESOLVED ANALYSIS

3.1. *Summary of Technique*

The GRBs in our sample were selected based on two criteria: large peak flux and single-peaked, non-overlapping temporal structure. The GRBs were binned temporally in an objective way described in Section 3.3 and spectral fits were performed on each time bin using four different photon models (Band, Band+blackbody, synchrotron, synchrotron+blackbody). When fitting synchrotron we compared the fits of slow-cooling and fast-cooling synchrotron. In many cases the fits from fast-cooling synchrotron completely failed. From these spectral fits a photon flux lightcurve was generated for each component and fitted with a pulse model to determine the decay phase of the pulse. We describe each step in the following subsections.

3.2. *Sample Selection*

To fully constrain the parameters of the fitted models, we selected GRBs with a requirement that the peak flux be greater than 5 photons s^{-1} cm^{-2} between 10 keV and 40 MeV. For the GBM analysis, the time-tagged event (TTE) data was used due to its high temporal and spectral resolution. It is important for our GRBs to have a simple, single-peaked lightcurve structure to avoid the overlapping of different emission episodes. While we cannot be sure that a weaker emission episode does not lie

beneath the main peak, the bursts we selected have no significant additional peak during the rise or decay phase of the pulse. These two cuts left us a sample of eight GRBs: GRB 081110A (McBreen et al. 2008), GRB 081224A (Wilson-Hodge et al. 2008), GRB 090719A (van der Horst 2009), GRB 090809B, GRB 100707A (Wilson-Hodge et al. 2010), GRB 110407A, GRB 110721A, (Tierney et al. 2011) and, GRB 110920A (Figure 3). GRB 081224A and GRB 110721A were both analyzed including the new LAT Low-Energy (LLE) data that provides a high effective area above 30 MeV for the analysis of short-lived phenomena, thanks to a loosened set of cuts with respect to LAT standard classes (Pelassa 2009; Ackermann et al. 2012a). This data selection bypasses the typical photon classification (Ackermann et al. 2012c) tree and includes events that would normally be excluded but can be selected temporally when the signal to background rate is high, such as with GRBs. GRB 081224A had very little data above 30 MeV but the LLE data helped to constrain the spectral fits. From this sample, five GRBs (GRB 081224A, GRB 090719A, GRB 100707A, GRB 110721A, and GRB 110920A) had blackbody components that were bright enough to analyze (Table 1).

3.3. *Time Binning*

In order to bin the count data, the time bins for spectral analysis of each GRB were chosen using Bayesian blocks (Scargle et al. 2013). Bayesian blocks define the time bins by looking for significant changes in the data count rate that define change points based on a Bayesian prior. For GBM data, we combined the TTE data from the brightest NaI detector with the TTE data from the BGO detector and ran a Bayesian block algorithm to find the times of the change points. We found that a prior of 8 gave a good balance between time resolution and having enough counts to perform spectral analysis. These change points were mapped to the other detectors used in the analysis. This method only accounts for changes in counts and therefore could inadvertently combine bins with different spectral shapes.

3.4. *Spectral Analysis*

For spectral fits we used the RMFIT ver4.1[17] software package developed by the GBM team. Fitting the synchrotron photon model requires a custom module developed and used in B11. Each time bin was fit with one of the four spectral models mentioned above. An off pulse region was selected as background and fit with a polynomial in time for subtraction for both the TTE and LLE data. We fit the physical models to compare the validity of each one against the other and the Band function to try and understand how the Band function parameters correlate with the best fit physical model. If the addition of blackbody component did not make a significant improvement of at least 10 units of C-stat (Arnaud, Smith, & Siemiginowska 2011) for any time bins of a particular GRB, then we did not include the blackbody component in the analyzed fits for that burst. C-stat is a likelihood statistic that is modified by a constant that causes the statistic divided by the degrees of freedom to approach a χ^2 value to the limit of a large number of counts. However, near the end of the prompt emission in some GRBs, the blackbody component becomes weak but has spectral evolution consistent with more significant time bins in the burst. The spectral parameters of the blackbody in those bins were included even though they contributed large error bars to some quantities. We checked with simulations that this cut was sufficient to identify a significant addition of a blackbody to the fit model.

[17] http://fermi.gsfc.nasa.gov/ssc/data/analysis/user/

4. RESULTS

4.1. *Test of Slow-Cooling Synchrotron*

In nearly all cases the synchrotron or synchrotron+blackbody model produced a fit with a comparable or better C-stat than the Band function. The GRBs exhibited hard to soft spectral evolution (Figure 4) for both components. From these fits we can derive several interesting properties of the bursts. The results of fitting the non-thermal part of each time bin in our sample with slow-cooled synchrotron indicate that this model can indeed fit the data well. The C-stat fit statistic per degree of freedom was at or near 1 for most time bins. The spectral fit residuals cluster around zero, with no deviations at low-energy that might indicate an additional power-law component (Figure 5). The residuals are below 4σ for the entire energy range. As an example, the fit C-stats for GRB 100707A and GRB 110721A are shown in Tables 2 and 3 respectively. They show that the slow-cooled synchrotron model fits the data as well as the Band function when a blackbody is included. The fit C-stats for fast-cooled synchrotron are shown for GRB 110721A to compare all three non-thermal models. These results imply that slow-cooled synchrotron is a viable model for GRB prompt emission. We cannot claim it provides a better fit to the data than other untested models and we will investigate and compare other physical models in future work

An important parameter constrained in these fits is the electron index, δ, of the accelerated power-law. The canonical value from relativistic shock acceleration is δ=2.2 (Kirk & Schneider 1987; Kirk et al. 2000). The distribution of constrained δ's (Figure 6) is broad and centered around δ=5. This steep index could provide clues for the structure and magnetic turbulence spectrum of the shocks. Baring (2006) shows that shock speed, obliquity, and turbulence all have a strong effect on the electron spectral index of the accelerated electrons. Steeper indices correspond to increasing shock obliquity. Fit models which are built from the electron distribution such as the one used in this work enable a direct diagnostic of the GRB shock structure.

4.2. *Test of Fast-Cooling Synchrotron*

In order to see if any spectra were consistent with the fast-cooling synchrotron spectrum, we implemented a fast-cooled synchrotron model where the electrons were distributed according to the broken power-law in eq. 10. As with the slow-cooling fits, $\gamma_{\min}$ was held fixed to 30. Several spectra were tested and all resulted in very poor fits regardless of whether the low-energy index found with the Band function was much harder than $-3/2$ (Figure 7 and Table 4). This is due to the broad spectral

curvature of the fast-cooled spectrum around the νF_ν peak. The broken power-law nature of the electron distribution is smeared out by the synchrotron kernel and cannot fit the typical curvature of the GBM data. In fact, the fast-cooling synchrotron spectrum has a spectral index of $-2/3$ below the γ_c which we have fixed at 1. The fitting algorithm increased E_* to high values to align the $-2/3$ index with the data, which resulted in poor fits (Figure 8). Even when a blackbody is present in the bursts, fast-cooled synchrotron is not a good fit to the non-thermal part of the spectrum (Table 3). The lack of GRBs with low-energy indices as steep as $-3/2$, additionally disfavors fast-cooled synchrotron as the non-thermal emission component in GRB spectra.

4.3. *Synchrotron vs. Band*

The Band function has been used in the literature as a proxy for distinguishing among non-thermal emission mechanisms. The predicted non-thermal emission of GRBs is typically characterized as a smoothly-broken power-law with the high-energy spectral index related to the index of accelerated electrons and the low-energy index related to the radiative emission process. Therefore, fitting a Band function to the emission spectrum of a GRB *should* serve as a diagnostic of the radiative process responsible for the emission. Preece et al. (1998) examined the BATSE GRB catalog and looked at the distribution low-energy indices from Band function fits. They found that the distribution peaked at $\alpha \approx -1$ and that 1/3 of the fitted spectra had low-energy indices too hard for synchrotron radiation. The assumption is that the Band function's shape approximates synchrotron but has an added degree of freedom in the low-energy index. However, the Band function has a broader range of curvatures around the νF_ν peak allowing it the possibility to deviate from the shape of synchrotron above and around the νF_ν peak. The synchrotron νF_ν peak is $\propto \gamma_{\rm min}^2 B \propto E_*$, leading to the relation between Band and synchrotron models $E_{\rm peak} \propto E_*$. This relationship is easily recovered from our sample (Figure 9). Direct comparison of the quality of the fits using Band and the synchrotron model is not the goal of this study. Both Band and the synchrotron model fit the data well with their respective fit residuals not deviating more than 4σ and centered around zero (Figure 5). It is important to stress that the questions being asked are does the synchrotron model fit the data? and, what temporal evolution do the synchrotron parameters undergo?

For all GRBs in our sample that include both a blackbody and non-thermal component we compare the photon flux (photons s^{-1} cm^{-2}) lightcurves (integrated from 10 keV - 40 MeV) derived from synchrotron fits with those derived from Band fits (Figure 10). It is seen that while both methods recover the same total flux, the flux from the individual components is much better constrained when using the synchrotron model for the non-thermal component. This is due to the pliability of the Band function below $E_{\rm peak}$ that is not afforded to the synchrotron model.

The C-stat fit values for the synchrotron model loosely correlate with the value of Band α found by fitting the same interval with the Band function. When Band α was much harder than zero, the synchrotron fit was poor and typically required adding blackbody to fit the data. The flexibility of the Band function with its low-energy power law creates the possibility that the index alpha of that power law will not accurately measure the true slope if $E_{\rm peak}$ is too close to the low-energy boundary of GBM data. Simulated spectra using the Band function were created with a grid in both Band α and $E_{\rm peak}$ to ensure that low values of $E_{\rm peak}$ do not affect the reconstruction of Band α in our fits. It was found that Band α could be accurately measured when $E_{\rm peak}$ was as low as $\sim$20 keV. While the asymptotic value of synchrotron is $-2/3$, fitting the photon model with an empirical function like Band with a slightly different curvature could result in measured low-energy indices that are different. To measure this effect, simulated synchrotron spectra with different E_* were fit with the Band function. The Band α showed a slight dependence on the synchrotron peak; moving to softer values for lower E_*. The distribution of fitted Band α values from these simulations centered around -0.81 ± 0.1, a slightly softer value than $-2/3$ which may explain the clustering of Band α at -0.82 in the GBM spectral catalog (Goldstein et al. 2012a) if a majority of the non-thermal spectra are the result of synchrotron emission.

4.4. *High-Energy Correlations*

There is a well-known spectral evolution in GRB pulses of $E_{\rm peak}$ evolving from hard to soft (see Figures 3 and 4). This leads to two time-resolved correlations between hardness (measured as $E_{\rm peak}$) and flux (Golenetskii et al. 1983; Liang & Kargatis 1996; Ghisellini et al. 2010). Liang & Kargatis (1996) (hereafter LK96) showed that the hardness intensity correlation (HIC) which relates the instantaneous energy flux F_E to spectral hardness and can be defined as

$$F_E \;=\; F_0 \left(\frac{E_{\rm peak}}{E_{\rm peak,0}}\right)^q \qquad (15)$$

where F_0 and $E_{\rm peak,0}$ are the initial values at the start of the pulse decay phase and q is the HIC index. Borgonovo & Ryde (2001) found that 57% of a sample of 82 BATSE GRBs were consistent with this relation. The second relation is the hardness-fluence correlation (HFC) which relates hardness to the time-running fluence of the GRB. Time-running fluence, $\Phi(t)$, is defined as the cumulative, time-integrated flux of each time bin in a GRB. The HFC is expressed as

$$E_{\rm peak} \;=\; E_{\rm peak,0} e^{-\Phi(t)/\Phi_0} \qquad (16)$$

where Φ_0 is the decay constant. LK96 noted that this equation is similar to the form of a confined radiating plasma. This should not be the case for optically-thin synchrotron. Upon differentiating eq. 16 it becomes apparent that the change in hardness is nearly equal to the energy density:

$$-\frac{dE_{\rm peak}}{dt} \;=\; -\frac{F_\nu E_{\rm peak}}{\Phi_0} \;\approx\; -\frac{F_E}{\Phi_0}. \qquad (17)$$

The HFC could be the result of a confined plasma with a fixed number of particle cooling via γ-radiation as proposed by LK96. Since these relations are only valid during the decay phase of a pulse the value of T_{max} (the time of the peak flux) from the pulse fit of each GRB is used as the initial point for F_0 and $E_{\rm peak,0}$.

The use of a hardness indicator is somewhat ambiguous. Historically, the ratio of counts in low and high-energy channels was used as a hardness measure. This has an advantage of being model-independent but suffers from the lack of information associated with the instrument response. High-energy photons can scatter in the detector and not deposit their full energy thereby artificially lowering the hardness ratio. LK96 used the Band function E_{peak} to compute hardness, which as a deconvolved quantity is less instrument-dependent but introduces a model dependence. We take this approach for both the Band and synchrotron model fluxes. For synchrotron we use the E_* parameter as our hardness indicator. This is justified by the relationship between E_* and E_{peak} (see Sec. 4.3 and Figure 9).

We compute the HIC and HFC for the synchrotron fits for each GRB in our sample (Figure 11 and Table 5). All the GRBs seemed to follow the HIC to some extent. We find that the HIC index for E_* ranges between ≈1-2, with 1 being expected if the emission is due to synchrotron. When using the Band function E_{peak} as a hardness indicator, it is expected that $E_{peak} \propto L^{1/2} \propto F_E^{1/2}$ from basic synchrotron theory (Ghisellini et al. 2010). The synchrotron fits seem to obey the HFC fairly well. Owing to the large errors in the Band flux, fits with synchrotron are more consistent with the HFC and HIC than those with Band. The deviations of the data from the expected synchrotron HIC may be due to the fact that there are overlapping pulses under the main emission that alter the decay profile. In addition, the use of Bayesian blocks to select time bins ignores spectral evolution. If bins with very different E_{peak} are combined then it could affect the the HIC and HFC data.

4.5. *Blackbody component*

For most of the spectra in our sample, the blackbody's νF_ν peak is below the νF_ν peak of the non-thermal component. There is sometimes a much larger change in C-stat between fits with synchrotron and synchrotron+blackbody than those of Band and Band+blackbody owing to the fact that the Band function has more freedom in the shape below E_{peak} (Tables 6 and 7). Simulations of both Band and slow-cooling synchrotron were used to find the significance of adding a blackbody to the spectrum. It was found that even when the difference in C-stat between Band and Band+blackbody was greater than the difference between synchrotron and synchrotron+blackbody, the statistical significance in the goodness of fit after the addition of the blackbody as high if not greater for the synchrotron+blackbody model for many cases. Computational time limits kept us from checking if the significance reached 5σ. We now focus on the blackbody component that is found in the synchrotron+blackbody fits. The blackbody appears to have a separate temporal structure from the non-thermal component, typically peaking earlier in time and decaying before the non-thermal emission. (Figure 10).

The form of the blackbody used in this work (eq. 11) is simplified and therefore will likely only approximate the true form of thermal emission from a GRB photosphere. Since the blackbody is weaker than the non-thermal (synchrotron) component in the spectrum, the effects of a broadened and more realistic relativistic blackbody are masked and only slightly affect the fit when combined with the synchrotron model. However, in the case of GRB 100707A, the blackbody is very bright (Figure 10(c)) and subtle changes in actual shape of the photospheric emission become more apparent. This is reflected in the C-stat values in Table 2. The Band function combined with the standard blackbody is a better fit than when using synchrotron as the non-thermal component. In this case, the Band function α is still very hard indicating that the Band function is making up for additional flux that the blackbody is not taking into account. To test this hypothesis, we fit the synchrotron model with an exponentially cutoff power-law to mimic a modified blackbody. We found that the fits were as good as the Band function combined with blackbody fits indicating that when the blackbody is bright compared to the non-thermal emission a more detailed model of the photospheric emission is needed to fit the thermal part of the spectrum.

For each time interval the energy flux (ergs s^{-1} cm^{-2}) ratio is calculated for the synchrotron and blackbody components and the sum of these is calculated to obtain the total flux ratio (see Table 8). We fit the ratio $(F_{bb}/F_{synch})(t)$ vs kT(t) to see if it follows the trend of eq. 12. None of the components in our subset followed a linear trend but the values of the slope were all unconstrained due to the high error in the energy fluxes. The HIC for the blackbody component is equivalent to eq. 13; however, nearly all the blackbodies had a HIC index of $q \approx 2$ (Figure 12(a)). These results confirm Ryde (2004) and Ryde and Pe'er (2009) who fit BATSE spectra with a combination of a blackbody and a power-law to account for the non-thermal component. Ryde et al. (2008) describes a toy model for the blackbody that allows a range of temperature indices related to the internal structure of the photosphere that may account for these results.

Another interesting quantity that can be obtained from the blackbody is the HFC. All GRBs in our blackbody subset had blackbodies consistent with the HFC (Figure 12(b)). The decay constants were all of similar value. Crider et al. (1999) noted that similar values of Φ_0 for non-thermal components arise as a consequence of a narrow parent distribution. A deeper investigation of a larger sample is required to assess if the same is true for the blackbody components.

The temporal evolution of kT for the blackbody of each burst appears to follow a broken power-law (Figure 13). The evolution is fit with the function derived in Ryde (2004) where we fixed the curvature parameter, δ, to 0.15. The coarse time binning derived from Bayesian blocks does not allow for the decay indices to be constrained for all the bursts but a small subset are close to $-2/3$, as expected (see Table 9). The temporal decay of the blackbody is different than the power-law decay of E_*, indicating a different emission component.

The $\mathcal{R}$ parameter was observed to increase with time for all the GRBs (Figure 14). There are breaks and plateaus in the trends that do not seem to correlate with the breaks observed in the evolution of kT or with the flux history of the blackbody. Ryde and Pe'er (2009) found that the evolution of $\mathcal{R}$ can be quite complex but mostly follows an increasing power-law that seems independent of the flux history even for very complex GRBs.

For those complex GRB lightcurves, it was found that analyzing different intervals of the overlapping pulses yielded an HIC index for the blackbody of $q \sim 4$ for each interval. In those intervals, $\mathcal{R}$ was approximately constant indicating the emission size of the photosphere was constant. Owing to the small number of time bins, it is difficult to quantify the evolution of $\mathcal{R}$ for the single pulse GRBs of this study with the coarse time binning used, but the fact that the HIC index for the blackbodies differs from $q \sim 4$ and that $\mathcal{R}$ increases indicates that the evolution of the photosphere is very complex.

5. DISCUSSION

5.1. *The Importance of Fitting with Physical Models*

With the use of physical emissivities in GRB spectroscopy we have shown that the *Fermi* data are consistent with synchrotron emission from electrons that have not cooled (i.e, slow-cooling spectra) and are inconsistent with synchrotron emission from electrons that are cooling (fast-cooling). The method enables us to test conclusions drawn from the empirical modeling that has dominated the field. There is a positive correlation between hard alpha and the inability of the data to fit the synchrotron model, but the low-energy index of synchrotron seems to center around -0.8 rather than the asymptotic $-2/3$ assumed in Preece et al. (1998). Not only do the fits with Band α centering around -0.81 lead to better fits with synchrotron, but simulated synchrotron spectra are best fit with a Band function having an $\alpha \approx -0.8$. This fact alone has very powerful implications for making physical interpretations from the value of Band function parameters.

Previously, GRB spectra have been successfully fitted with a thermal + non-thermal model , i.e., by using a blackbody function combined with a Band function. A thermal spectral component has indeed been shown to be significant in several cases, foremost in GRB 100724B and in GRB 110721A (Guiriec et al. 2011; Axelsson et al. 2012). The Band function in these fits is, however, not based on any physical arguments but is merely an empirical function that has a pliant parametrization. A general problem that arises in this type of fitting is that the low-energy slope of the Band function (α) and the strength of the blackbody are degenerate to varying degrees. When the data is fit by a Band function alone, even if an additional component really exists in the data at lower energies, it may not be identified because the α of the Band function can accommodate the additional low energy flux by changing its slope.

The slow-cooling synchrotron model we use here is more restrictive compared to the Band function. In particular, the low energy slope (α) and the curvature of the spectrum are predicted by the model.

The spectrum below the synchrotron νF_ν peak is not always satisfactorily fit using just the synchrotron model. The residuals suggest that an additional component is sometimes needed, and we use simulations to show that this additional component is statistically significant. Additional components can also be favored in GRBs fit with the Band function but we found that the significance of the additional component can be greater when added to the synchrotron fits than when added to the Band fits. We explain this by noting the Band function can accommodate the extra emission using a suitable power-law index α but the synchrotron function is more restrictive and the additional component is thus required to give a reasonable fit. Another essential observation is shown in Figure 10: when using the synchrotron model, the temporal evolution of the blackbody flux exhibits well-defined pulses and a spectral evolution that is clearly separated from the non-thermal emission. This is in contrast to the less smooth blackbody flux variations when using the Band function as the non-thermal process. This fact again reflects that the Band function is less restrictive than the synchrotron function and thereby gives rise to further scatter in the derived fluxes in the light curves. We also argue that these facts suggest that:

(i) the synchrotron function is a good physical model to use

(ii) the thermal component does exist and

(iii) multi-component fitting with the Band function can be misleading.

5.2. *Alleviating Slow-cooling Synchrotron Problems*

The fact that the non-thermal spectra seem to be consistent with slow-cooled synchrotron and not fast-cooled synchrotron places strong constraints on the emission model of GRBs. Ghisellini et al. (2000) showed that trying to reconcile fast-cooling with the observations leads to even further problems for the internal shock model. In our simple model of fast-cooled synchrotron, we neglected the effects of inverse-Compton cooling in the Klein-Nishina regime, which can significantly alter the value of the low-energy slope (Daigne, Bošnjak, & Dubus 2011). This could make some spectra consistent with fast-cooling, but the effect on the spectral curvature has not been assessed and therefore further investigation is required. Neglecting Klein-Nishina effects, the internal shock scenario cannot be reconciled with our observations. Additionally, Iyyani et al. (2013, in prep.) found that for GRB 110721A, the standard slow-cooling synchrotron scenario from impulsive energy input such as internal shocks places the non-thermal emission region below the photosphere. This calculation is possible due to the observation of the blackbody component, highlighting the importance of multi-component fitting.

Models with co-acceleration via first-order and second-order Fermi acceleration (Waxman 1995; Dermer & Humi 2001) have the ability to balance synchrotron cooling with stochastic heating keeping $\gamma_{\rm cool}$ above $\gamma_{\rm min}$. The spectrum would resemble a slow-cooled synchrotron spectrum. The internal-collisional-induced magnetic reconnection model (ICMART) (Zhang & Yan 2011) makes use of magnetic reconnection to accelerate electrons to high energies. Electrons are not accelerated just once. Instead they are constantly accelerated via second-order turbulence. This leads to a balance between cooling and acceleration, producing a synchrotron spectrum that is in the slow-cooling regime. In addition, the ICMART model extends the non-thermal emission site far above the photosphere which eliminates the problem mentioned above. While simulated spectra from

the ICMART model are currently under development (Bing Zhang, *private communication*), none have been published to be tested. Still, our analysis suggests that such slow-heating scenarios can explain the data much better than the current internal shock model.

5.3. *Conclusion*

We have demonstrated that for a set of GRBs we can fit a physical, slow-cooling synchrotron model directly to the data. Most spectra require a sub-dominant blackbody with a temperature that places its peak below the synchrotron νF_ν peak. The temporal evolution of both radiative components allows for the assessment of GRB jet proprieties without the assumptions required when fitting GRB spectra with empirical functions. Several parameters in our model can not be constrained by the fits, namely $\gamma_{\rm th}$, $\gamma_{\rm min}$, and B. Detailed assumptions about jet properties are required to specify these parameters which we will assess in future work. Still, the temporal evolution of both synchrotron and blackbody component imply that in these GRBs, a photosphere is formed below a non-thermal emitting region that forms at a larger radius than the classical internal shock scenario. The electrons in the non-thermal emitting region must undergo continuous acceleration to produce a slow-cooling synchrotron spectrum. These findings help to prune the numerous models of GRB emission and provide impetus for the further use of physical fitting models.

We would like to thank Frédéric Daigne and Bing Zhang for helpful discussions concerning the nature of the non-thermal emission.

The *Fermi* LAT Collaboration acknowledges generous ongoing support from a number of agencies and institutes that have supported both the development and the operation of the LAT as well as scientific data analysis. These include the National Aeronautics and Space Administration and the Department of Energy in the United States, the Commissariat à l'Energie Atomique and the Centre National de la Recherche Scientifique / Institut National de Physique Nucléaire et de Physique des Particules in France, the Agenzia Spaziale Italiana and the Istituto Nazionale di Fisica Nucleare in Italy, the Ministry of Education, Culture, Sports, Science and Technology (MEXT), High Energy Accelerator Research Organization (KEK) and Japan Aerospace Exploration Agency (JAXA) in Japan, and the K. A. Wallenberg Foundation, the Swedish Research Council and the Swedish National Space Board in Sweden.

Additional support for science analysis during the operations phase is gratefully acknowledged from the Istituto Nazionale di Astrofisica in Italy and the Centre National d'Études Spatiales in France.

REFERENCES

Ackermann, M. et al., 2012, ApJ, 745, 144.
Ackermann, M. et al., 2012, ApJ, 754, 121.
Ackermann, M. et al., 2012, ApJS, 203, 4.
Arnaud K., Smith, R., & Siemiginowska, A. 2011, Handbook of X-ray Astronomy (Cambridge University Press)
Axelsson, M. et al. 2012, ApJ, submitted (arXiv:1207.6109)
Asano, K., Inoue, S., Mészáros, P. 2009, ApJ, 699, 953.
Band, D., Matteson, J., Ford, L., & Schaefer, B. 1993,ApJ, 413, 281.
Baring, M. G., Ellison, D. C., & Jones, F. C. 1995, Adv. Space. Res., 15, 397.
Baring, M. G. & Braby, M. 2004, ApJ, 613, 460.
Baring, M. G., 2006, Adv. Space. Res., 38, 1281.
Baring, M. G. 2011, Adv. Space. Res., 47, 1427.
Beloborodov, A. M. 2010, MNRAS, 407, 1033.
Beloborodov, A. M. 2012, (arXiv:1207.2707)
Blumenthal, G. R. & Gould, R. J. 1970, Phys. Rev. 42, 237.
Bošnjak Ž., Daigne F. & Dubus G. 2009, Astron. Astrophys., 498, 677.
Borgonovo, L. & Ryde F. 2001, ApJ, 548, 770.
Burgess, J. M. et al. 2011 ApJ, 741, 24.
Cavallo, G. & Rees, M. 1978, MNRAS, 183, 359.
Cenko et al. 2011, ApJ, 732, 29.
Cohen, E. et al. 1997, ApJ, 488, 330.
Crider, A. et al. 1999, ApJ, 519, 206.
Daigne, F. & Mochkovitch R. 1998 M.N.R.A.S., 296, 275.
Daigne, F. & Mochkovitch, R. 2002 M.N.R.A.S., 336, 1271.
Daigne F., Bošnjak Ž., & Dubus, G. 2011, Astron. Astrophys., 526, A110.
Dermer, C. & Humi, M. 2001, ApJ, 556, 479.
Goldstein A. et al. 2012, ApJS, 199, 19.
Goldstein A. et al. 2012, ApJS, *submitted*
Golenetskii, S., et al 1983, Nature 306, 1983.
González M. et al. 2003, Nature, 424, 749.
Goodman, J. 1986, ApJ, 308, L47.
Ghisellini et al. 2000, M.N.R.A.S., 313, L1.
Ghisellini et al. 2010, M.N.R.A.S., 403, 926.
Guiriec, S., et al. 2010, ApJ, 725, 225.
Guiriec, S., Connaughton, V., Briggs, M., & Burgess, M., et al. 2011, ApJ, 727, L33.
Guiriec, S., Daigne, F., Hascoët, R., et al. 2012, arXiv:1210.7252
Kirk, J. & Schneider, P. 1987, ApJ, 315, 425.
Kirk, J. et al. 2000, ApJ, 542, 235.
Liang, E. & Karagtis, V. 1996, Nature, 381, 49.
McBreen, S. et al. 2008, GCN Circular 8519
Meegan, C., et al. 2009, ApJ, 702, 791.
Mészáros, P. & Rees, M. 2000, ApJ, 530, 292.
Mészáros, P. 2001, Science, 291, 79
Mészáros, P. 2002, AR & A, 40, 137.
Mészáros, P. 2006, Rep. Prog. Phys., 69, 2259.
Paczyński B. 1986, ApJ, 308, L43.
Pe'er, A. & Waxman, E. 2004, ApJ, 613, 48.
Pe'er, A. & Ryde, F. 2011, ApJ, 732, 49.
Pelassa V. et al. 2009, Proceedings for the 2009 Fermi Symposium. eConf Proceedings C091122, arXiv:1002.2617
Piran, T. 1999, Phys. Rep. 314, 575.
Preece, R., Briggs, M. S., Giblin, T., & Mallozzi, R. 2002, ApJ, 581, 1248.
Preece, R., et al. 1998, ApJ, 506, L23.
Rees, M. J. and Mészáros, P. 2005, ApJ, 506, L23.
Rybicki, G. & Lightman, A. 1979, Radiative Processes in Astrophysics (New York, Wiley and Sons)
Ryde, F. 2004, ApJ, 614, 827.
Ryde, F. 2005, ApJ, 625, L95.
Ryde, F. et al. 2008, ApJ, 652, 1400.
Ryde, F. and Pe'er, A. 2009, ApJ, 702, 1211.
Ryde, F. et al. 2010, ApJ, 709, L172.
Sari, R., Piran, T., & Narayan, R. 1998, ApJ, 497, 17.
Scargle, J. D. et. el 2013, ApJ, 764, 167.
Spitkovsky, A. 2008, ApJ, 682, L5.
Summerlin, E. J. & Baring M. G. 2012, ApJ, 745, 63.
Tavani, M. 1996, Phys. Rev. Lett. 76, 3478.
Tierney et al.2011, GCN Circular 12187
Horst, A. ,vd. 2009, GCN Circular 9691
Waxman, E. 1995, Phys. Rev. Lett., 75, 386.
Wilson-Hodge, C. et al. 2008, GCN Circular 8723
Wilson-Hodge, C. et al. 2010, GCN Circular 10944
Zhang, B. & Pe'er, A. 2009, ApJ, 700, L65.
Zhang, B. & Yan, H. 2011, ApJ, 726, 90.
Zhang, B. et al. 2012, ApJ, 758, L34.

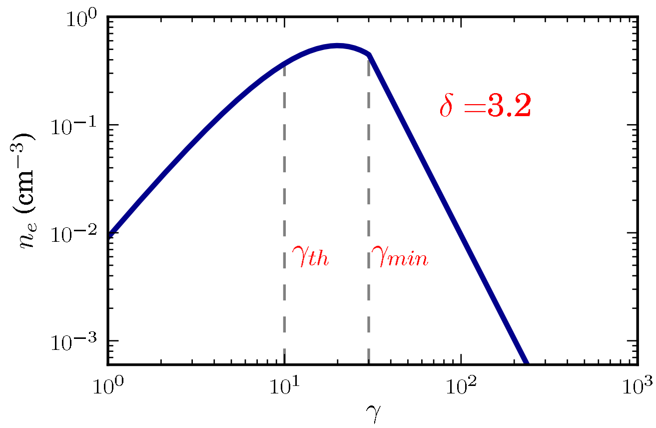

Figure 1. The physical electron spectrum used for fitting synchrotron spectra directly to the data. Here $\gamma_{\rm th} = 10$ and $\gamma_{\rm min} = 30$ which are the fixed values used for all fits in this study.

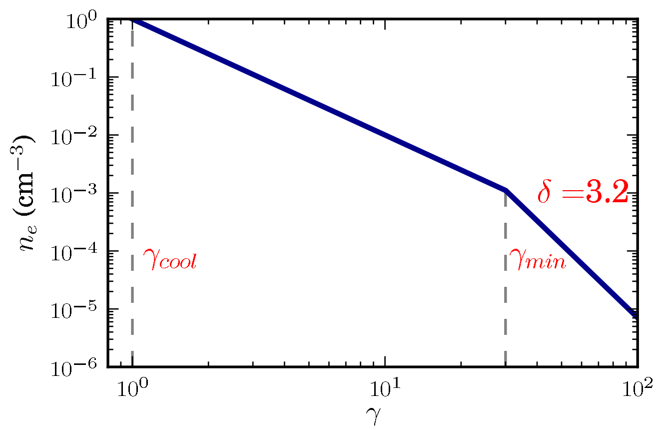

Figure 2. The fast-cooled electron distribution with $\gamma_{cool} = 1$ and $\gamma_{\rm min} = 30$. A low-energy thermal distribution is excluded in this distribution because the synchrotron emission from the power-law form is already too broad for the typical νF_ν peak of the data and including a thermal distribution would smooth it further.

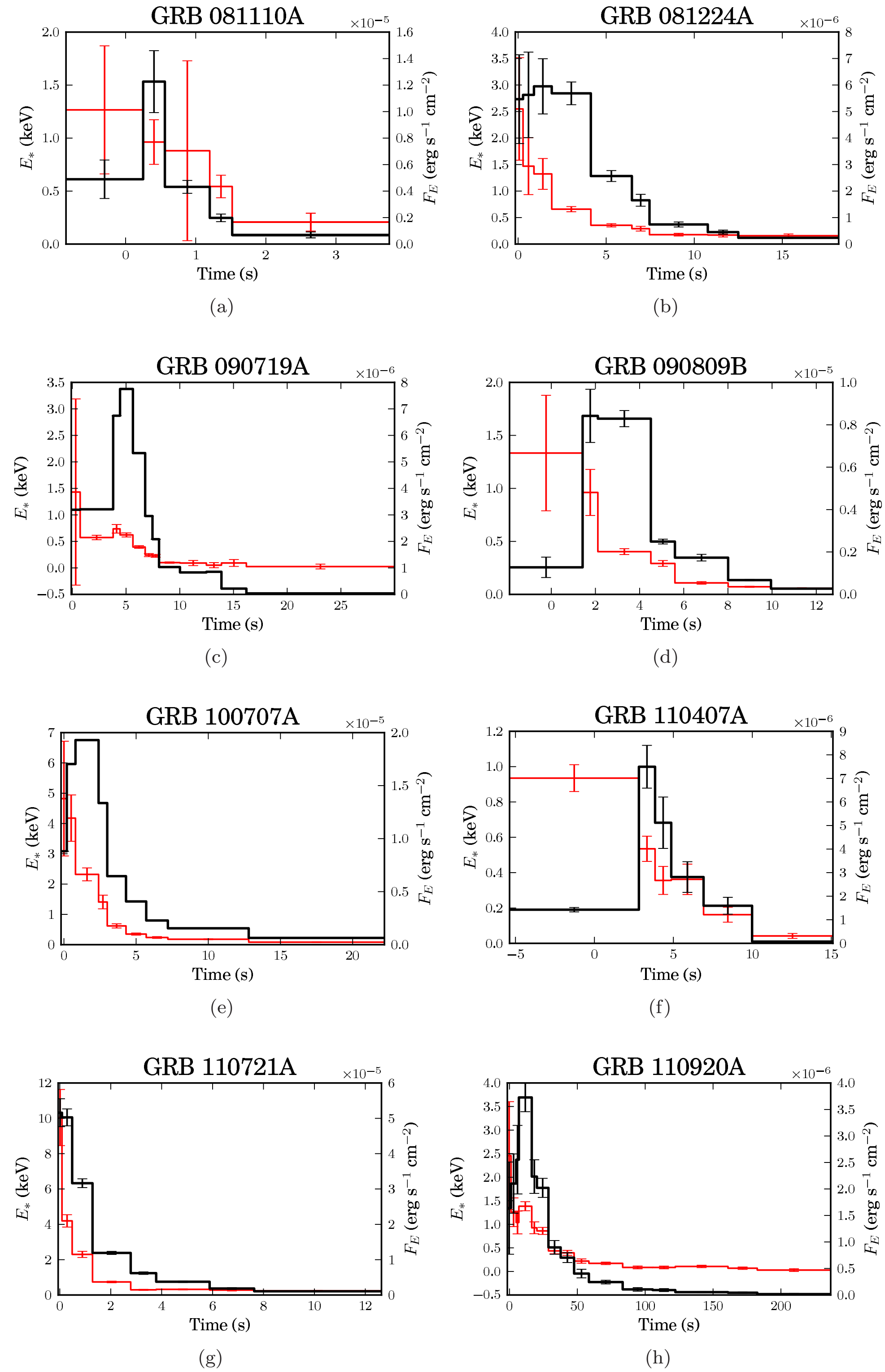

Figure 3. The energy flux lightcurves of the synchrotron component for the entire sample (*black* curve). The integration range is from 10 keV - 40 MeV for all GRBs except GRB 081224A and GRB 110721A which are from 10 keV - 300 MeV. Superimposed is the slow-cooled synchrotron E_* (see eq. 5) (*red* curve) demonstrating the hard to soft evolution of the bursts.

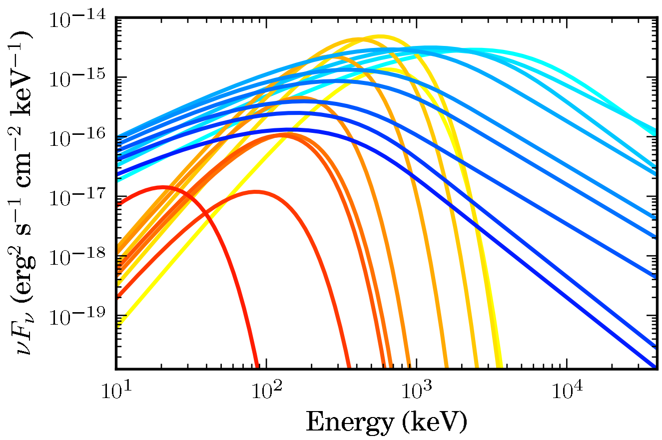

Figure 4. The spectral evolution of GRB081224A is an example of the typical evolution observed for the entire sample. The synchrotron (from *light blue* to *dark blue*) and blackbody (from *yellow* to *red*) both evolve from hard to soft peak energies with time. For this GRB, the high-energy power-law corresponding to the electron spectral index does not evolve significantly over the duration of the burst.

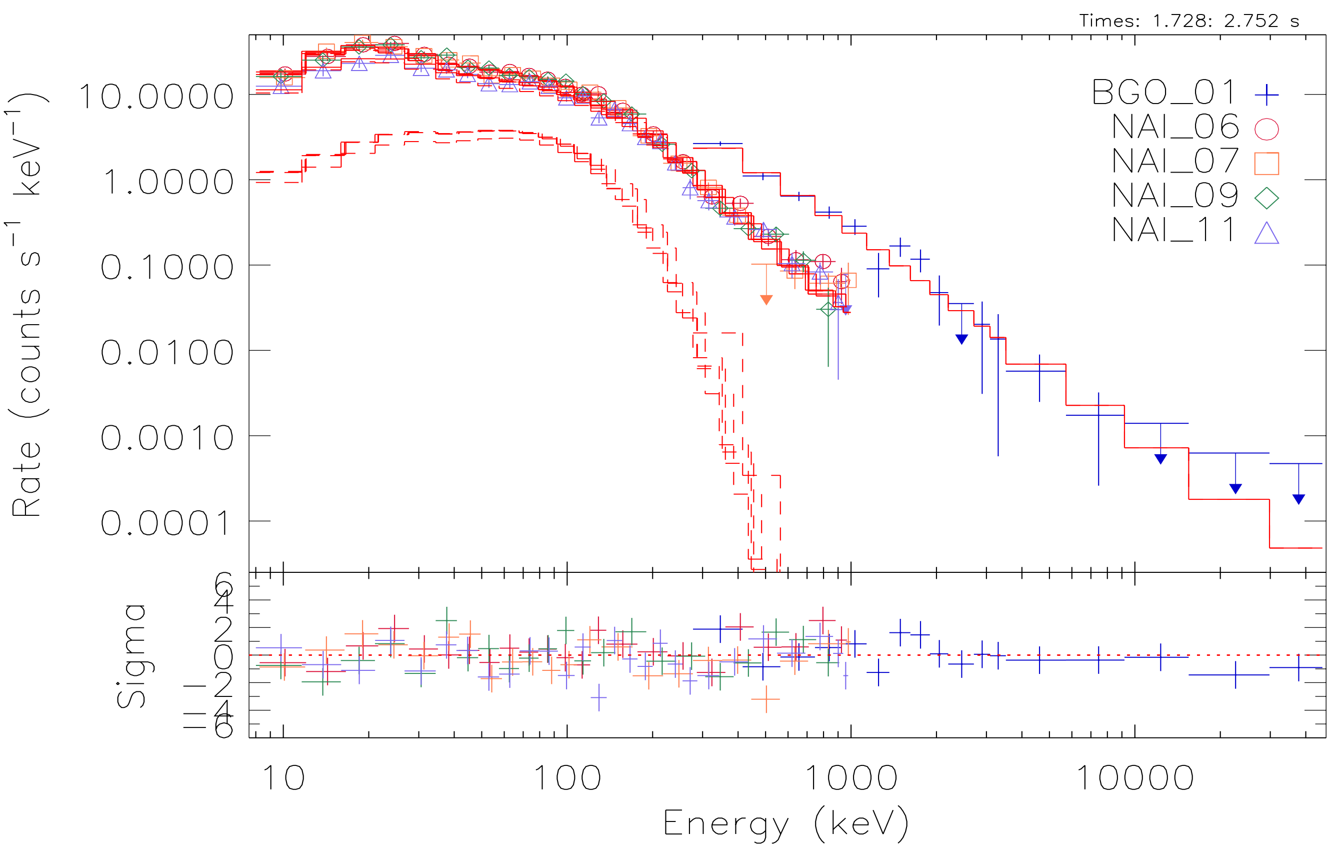

Figure 5. A time bin of GRB 110721A demonstrating a typical count spectrum of a time bin in the sample. The response has been convolved with synchrotron (eq 3) and a blackbody to produce counts. The residuals from the fit indicate that the model is fitting the data well.

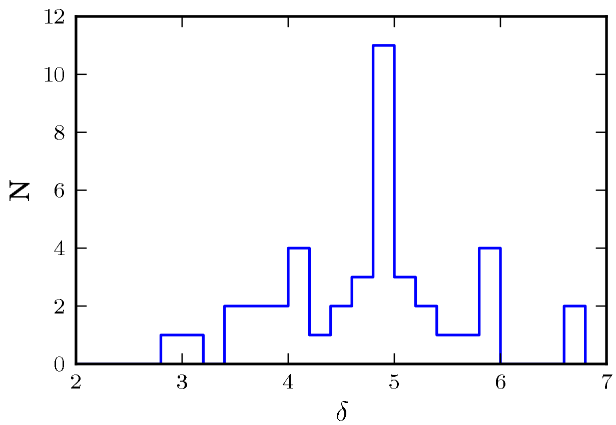

Figure 6. The distribution of electron indices from the slow-cooling synchrotron fits. Only indices that were constrained are plotted. The distribution is broad but centered at δ =5 which is much steeper than expected from simple relativistic shock acceleration.

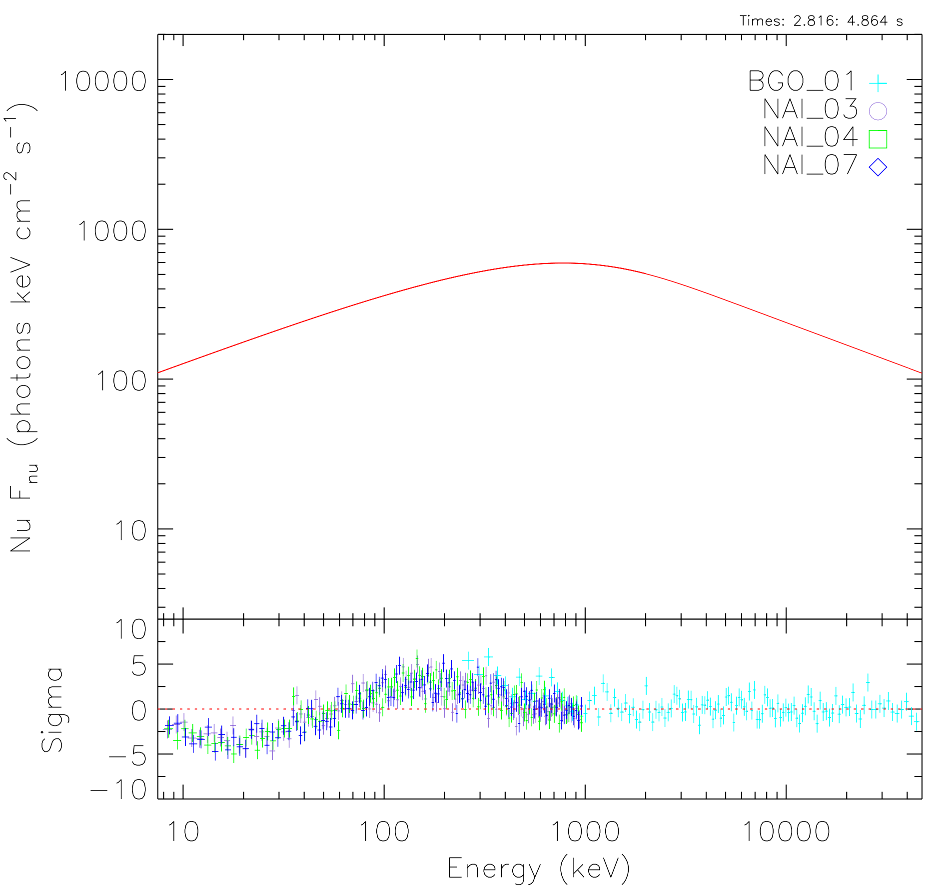

Figure 7. The fast-cooled synchrotron fits are poor for nearly all of our sample because none of the spectra have a low-energy index as steep as $-3/2$. Therefore the fast-cooled synchrotron spectrum is too broad around the νF_ν peak as shown in this example spectrum.

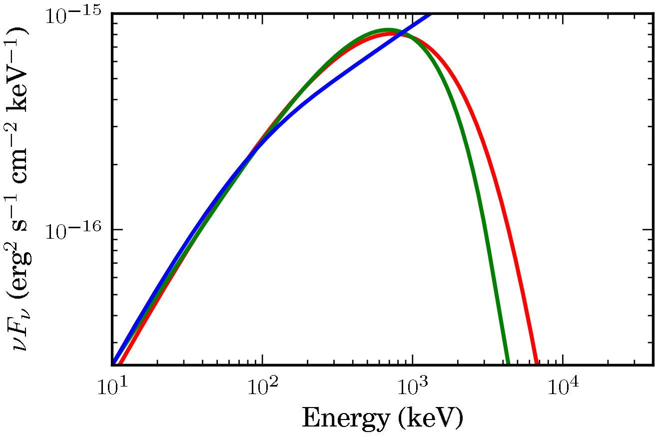

Figure 8. An example time bin of GRB 110407A comparing the fitted νF_ν spectra of the Band Function (*green*), slow-cooled synchrotron (*red*), and fast-cooled synchrotron (*blue*). While the Band function and slow-cooled synchrotron fits resemble each other, the fast-cooled synchrotron fit is only able to fit the low-energy part of the spectrum. Because fast-cooled synchrotron has an index of $-2/3$ below the cooling frequency, the fitting engine pushes the value of E_* very high to fit the low-energy part of the spectrum resulting in a $-3/2$ index near the νF_ν peak. The high-energy power-law of the fast-cooling synchrotron spectrum is pushed out of the data energy window.

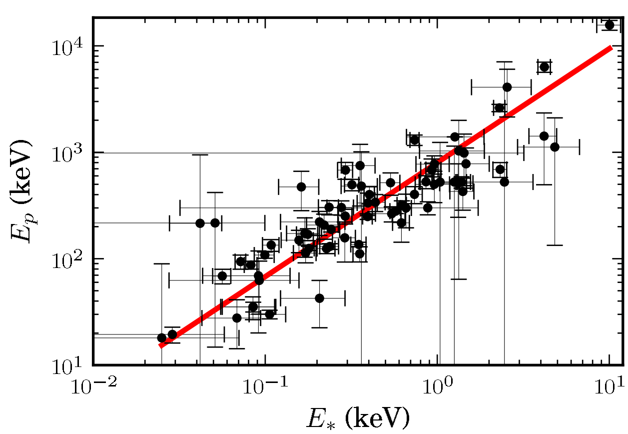

Figure 9. Derived values of the parameter $E_{\rm peak}$ (obtained using the Band function to fit GRB spectra), versus E_* (obtained using an optically-thin non-thermal synchrotron to fit GRB spectra).

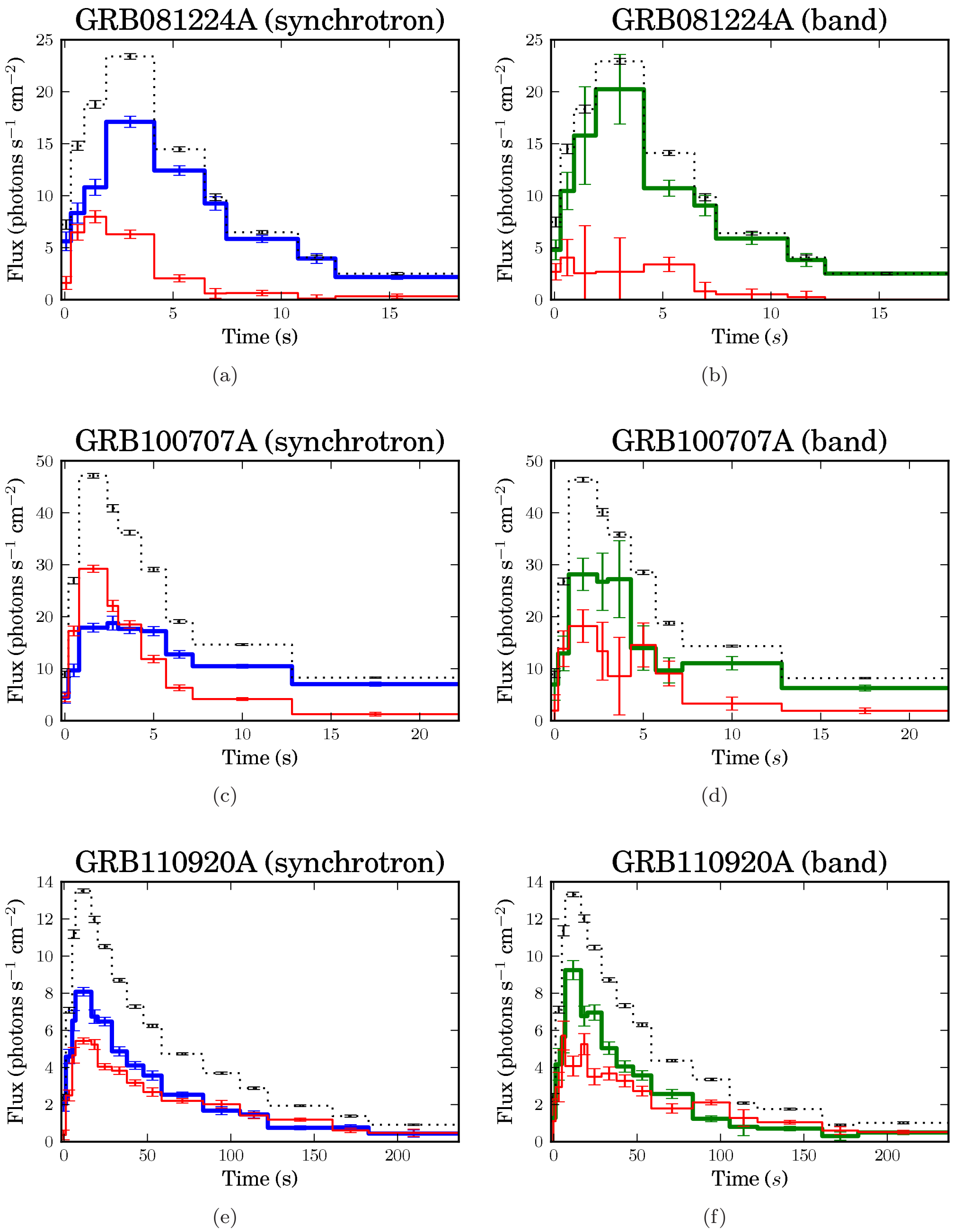

Figure 10. A subset of flux lightcurves illustrating both the temporal structure of the different components and the advantages of using a physical model to deconvolve the detector response. The left column contains the lightcurves using synchrotron (*blue thick line*) and blackbody (*red thin line*) while the right column contains the lightcurves made from using the Band function (*green thick line*) and blackbody (*red thin line*). The total flux lightcurve (*black dotted line*) of both approaches are the same. The components have a very simple and constrained evolution when using synchrotron as the non-thermal component. This is potentially indicative that synchrotron is the actual emission mechanism and the response is being properly deconvolved. In contrast, the lightcurves where the Band function is used have large errors and the blackbody does not have a consistent evolution. (See the online version for color)

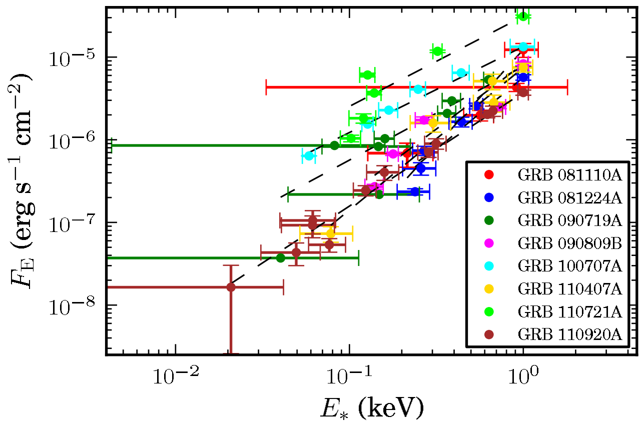

(a)

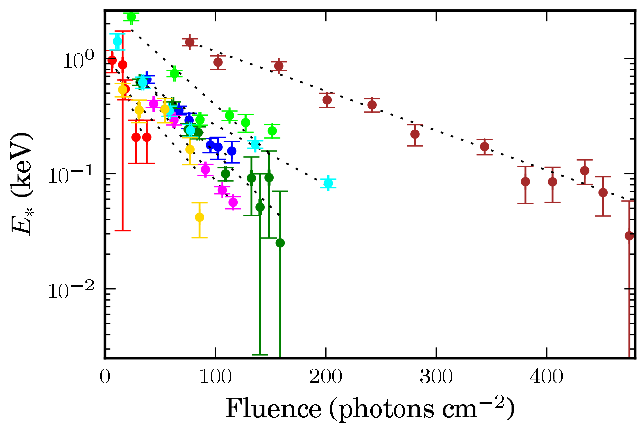

(b)

Figure 11. The non-thermal emission of all of the bursts in the sample loosely follow F_E-E_* and E_*-fluence relations. For synchrotron, the index of this relation should be 1. See Table 5 for the numerical results.

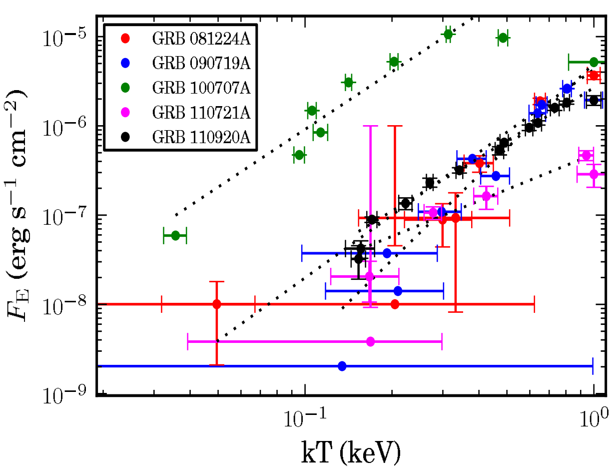

(a)

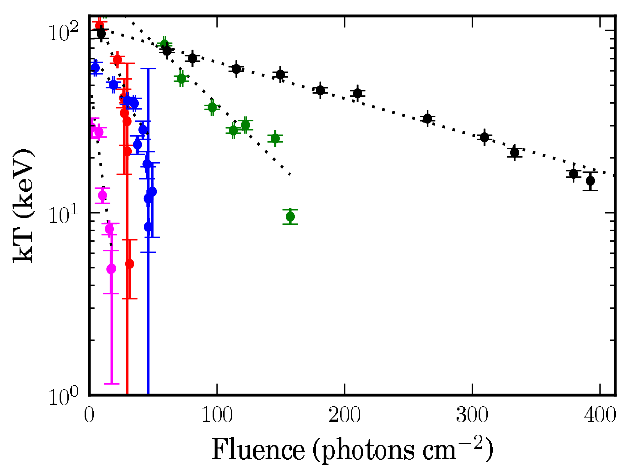

(b)

Figure 12. The HIC and HFC correlations for the blackbody are separate from those derived from the synchrotron component. This adds more evidence for the presence of the component. However, the HIC for the blackbody is not q=4 as expected.

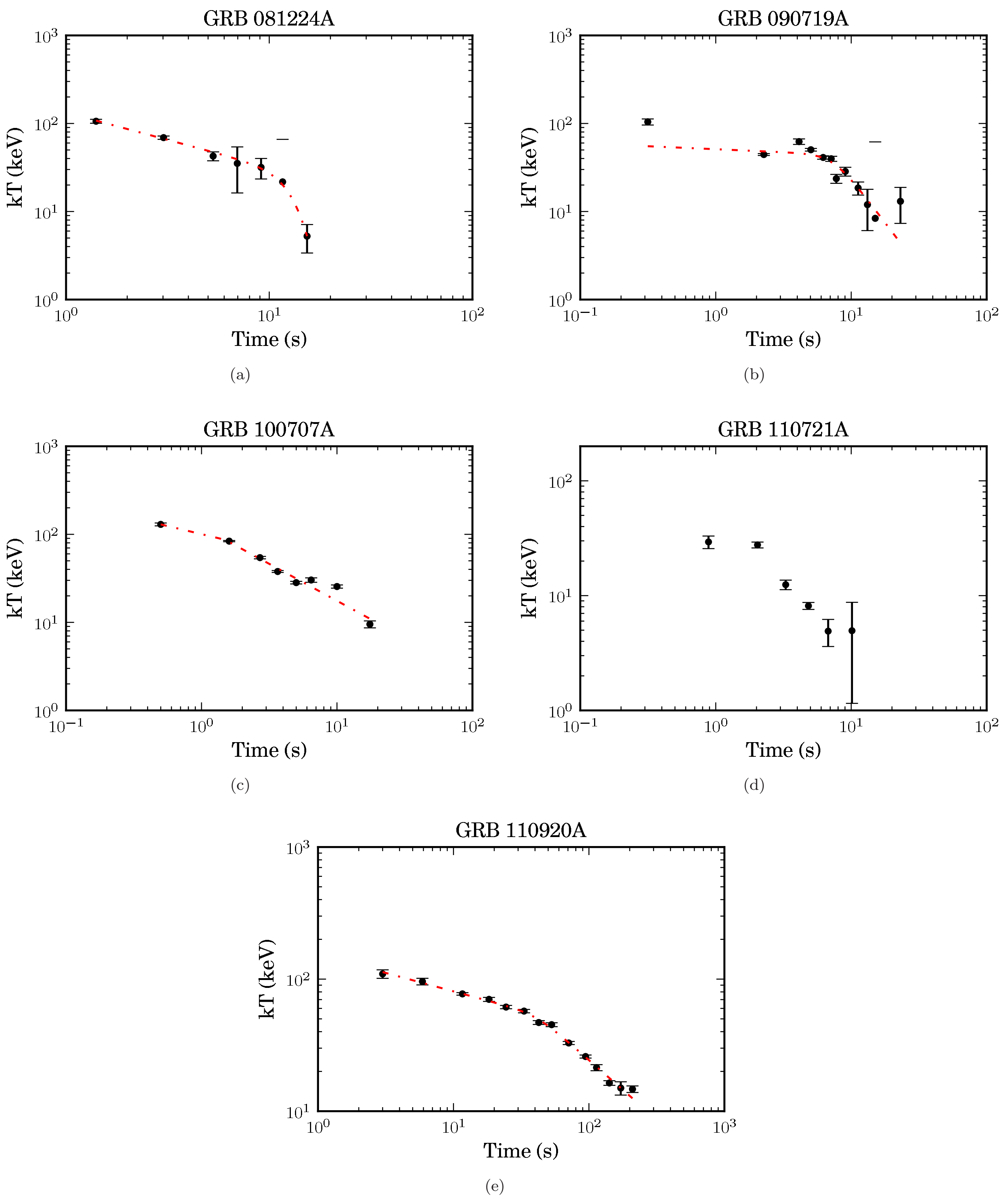

Figure 13. The time evolution of kT for four of the GRBs in our sample. GRB110721A is shown without a fit because the coarse time binning used did not allow for constraining the fit parameters. However, in Axelsson et al. (2012), the evolution is shown to follow a broken power-law.

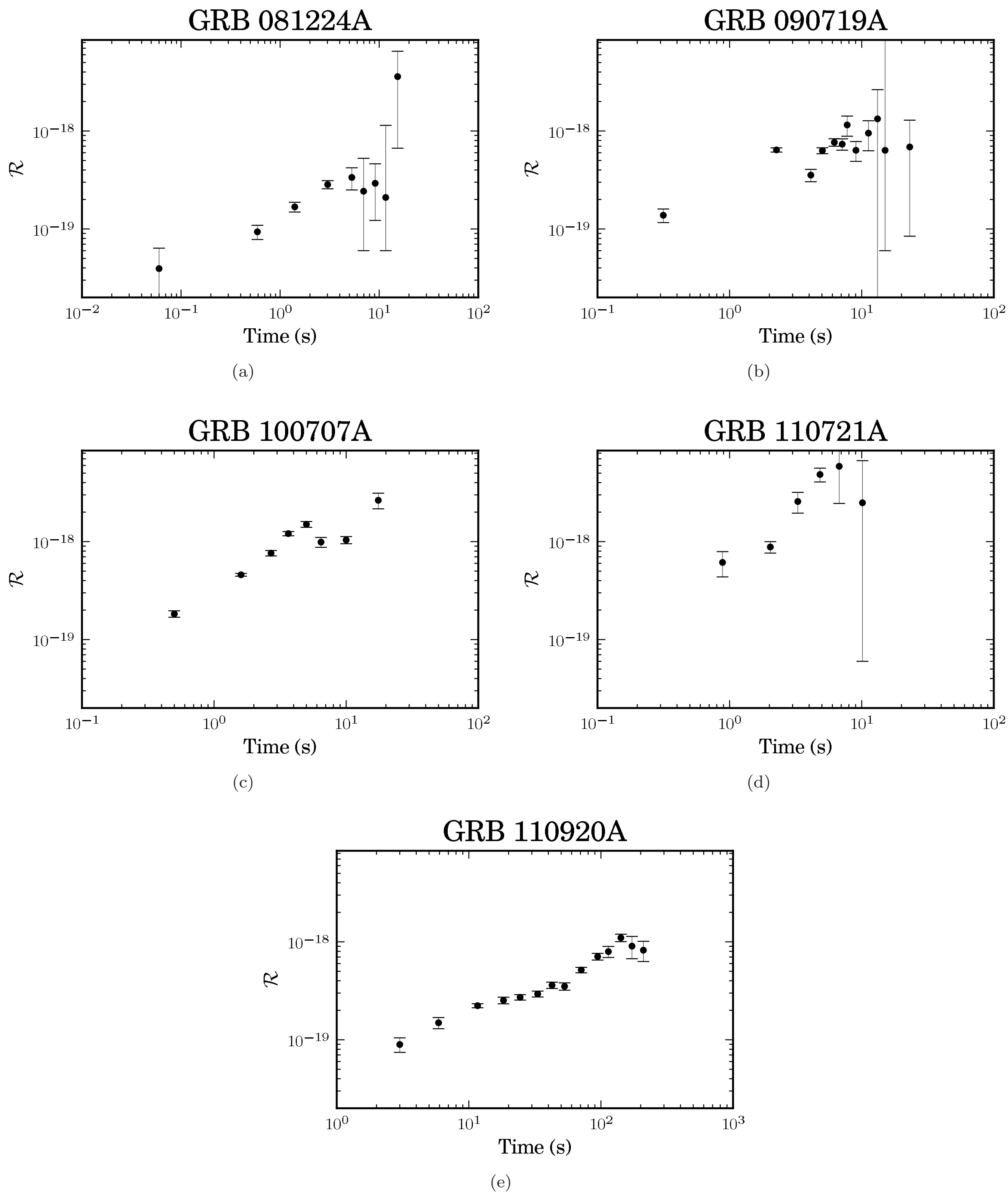

Figure 14. The evolution of the $\mathcal{R}$ parameter is increases with time and shows no relation to the photon flux of the blackbody component.

GRB	Peak Flux (p/s/cm^2)	Duration Analyzed (s)	Blackbody Component	LLE data
GRB 081110A	20.88	4.61	X	X
GRB 081224A	17.11	18.36	✓	✓
GRB 090719A	26.52	30.09	✓	X
GRB 090809B	18.36	14.64	X	X
GRB 100707A	18.77	22.39	✓	X
GRB 110407A	15.6	20.48	X	X
GRB 110721A	29.82	12.7	✓	✓
GRB 110920A	8.08	238.29	✓	X

Table 1
The GRBS in our sample. The peak fluxes were taken from the brightest bin of each GRB with a duration determined by Bayesian blocks.

Time Bin	Band C-Stat	Band+BB C-Stat	Synchrotron C-stat	Synchrotron+BB C-stat
-0.2-0.2	453	450	485	455
0.2-0.8	374	362	695	364
0.8-2.4	427	405	2546	487
2.4-3.0	408	400	903	413
3.0-4.3	431	415	1214	430
4.3-5.7	397	363	791	399
5.7-7.2	411	390	598	422
7.2-12.8	488	414	829	447
12.8-22.2	558	412	594	423

Table 2
The time-resolved C-Stat values for GRB100707A show that while the Band function and synchrotron models combined with a blackbody function both fit the data well, the non-thermal functions fit the data very differently when not combined with a blackbody. Specifically, where the blackbody is the brightest (Figures 10(c) and 10(d) intervals 2, 3, and 4) the Band function alone fits the data acceptably while the synchrotron model alone fits the data poorly. This shows that the flexibility of the Band function can mask the need for the blackbody component. The Band+blackbody fits actually fit the data better when the blackbody is very bright in this case. This is most likely due to the blackbody function (eq. 11) used is simplified and the actual emission may be broadened due to beaming effects that are only important to the fit when the blackbody is bright and the synchrotron fit is used. The Band function makes up for these effects by having a harder α. We tested using an exponentially cutoff power-law combined with the synchrotron model and the fits were as good as those with the Band function. We will examine the use of a more realistic photosphere model in future work.

Time Bin	Band C-Stat	Band+BB C-Stat	Synchrotron C-stat	Synchrotron+BB C-stat	Fast C-stat	Fast+BB C-stat
-0.07-0.08	640	640	673	673	709	709
0.08-0.48	690	690	704	704	1088	1088
0.48-1.28	709	668	688	670	1654	957
1.28-2.78	887	761	838	770	1646	1041
2.78-3.78	678	642	655	643	797	666
3.78-5.88	648	631	677	634	694	660
5.88-7.63	729	728	733	721	773	724
7.63-12.63	932	693	693	692	756	698

Table 3

The C-stat values for GRB 110721A. The significance of the addition of the blackbody is not as large as with GRB 100707A (Table 2) due to the weakness of the blackbody component. The fits for fast-cooled synchrotron are included to demonstrate the poor quality fits that are obtained both with fast-cooling synchrotron and fast-cooling synchrotron with a blackbody.

Time Bin	Band α	Slow-cooled Synchrotron C-stat	Fast-cooled Synchrotron C-stat	$\Delta_{\mathrm{C-stat}}$
-5.38-2.82	-0.9	523	599	76
2.82-3.84	-0.7	507	604	97
3.84-4.86	-0.8	506	596	90
4.86-6.91	-1.0	534	626	92
6.91-9.98	-1.1	591	639	48
9.98-15.1	-1.5	494	494	0

Table 4
For each time bin of GRB 110407A we examine the C-stat value of synchrotron and fast-cooled synchrotron. This GRB did not have a blackbody in its spectrum. While the Band function and slow-cooling synchrotron fit the spectrum well, fast-cooling synchrotron does not fit the spectrum unless Band $\alpha = -1.5$. In this case, the fast-cooled synchrotron peak energy was very unconstrained due to the curvature of the data being narrower than the photon model's curvature.

GRB	Flux Index	χ^2_{red}	Φ_0	χ^2_{red}
GRB 081110A	2.32±0.4	0.6	97±23	0.4
GRB 081224A	1.74±0.1	1.5	253±23	0.3
GRB 090719A	1.14±0.07	0.98	245±17	1.2
GRB 09080B	1.58±0.05	8.0	188±9	1.0
GRB 100707A	1.04±0.02	1.2	444±24	7.3
GRB 110407A	1.72±0.20	0.5	214±32	4.2
GRB 110721A	1.08±0.03	14.4	269±13	15.4
GRB 110920A	1.37±0.06	0.5	669±33	1.2

Table 5
Sample correlations for both flux and fluence for the synchrotron component.

Time Bin	Band-BB Δ_{C-stat}	Synchrotron-BB Δ_{C-stat}
-0.2-0.2	3	30
0.2-0.8	12	331
0.8-2.4	22	2059
2.4-3.0	8	490
3.0-4.3	16	784
4.3-5.7	34	392
5.7-7.2	21	176
7.2-12.8	74	382
12.8-22.2	146	171

Table 6
The Δ_{C-stat} between the Band function and synchrotron model fits with and without the inclusion of a blackbody for GRB 100707A. The blackbody has a significantly larger impact on the fit when included with the synchrotron model.

Time Bin	Band-BB Δ_{C-stat}	Synchrotron-BB Δ_{C-stat}	Fast-BB Δ_{C-stat}
-0.07-0.08	0	0	0
0.08-0.48	0	0	0
0.48-1.28	41	18	697
1.28-2.78	126	68	605
2.78-3.78	36	12	131
3.78-5.88	17	43	34
5.88-7.63	1	12	49
7.63-12.63	239	1	58

Table 7
The Δ_{C-stat} values for GRB 110721A tell a different story than GRB 100707A (Table 6), though both GRBs show a significant improvement in the fit when a blackbody is included. Even thought the fast-cooled fits showed extreme improvement with the inclusion of a blackbody, the fits are still poor compared with the slow-cooled model (See Table 3).

GRB	Flux Index	χ^2_{red}	Φ_0	χ^2_{red}
GRB 081224A	2.3 ± 0.3	1.4	121 ± 13	9
GRB 090719A	2.8 ± 0.4	2.3	232 ± 23	3
GRB 100707A	2.2 ± 0.1	17.4	319 ± 8	28
GRB 110721A	1.3 ± 0.2	1.8	43 ± 3	5
GRB 110920A	2.0 ± 0.1	0.9	1147 ± 21.7	4

Table 8
For the subset of bursts that have a strong blackbody component we compute the flux and fluence correlation for the blackbody.

GRB	F_{bb}/F_{syn}	1^{st} Decay Index	2^{nd} Decay Index	χ^2_{red}
GRB 081224A	0.3	-0.6 ± 0.07	-20 ± 243	0.5
GRB 090719A	0.4	-0.1 ± 0.05	-2.0 ± 0.7	11.3
GRB 100707A	0.5	-0.4 ± 822749	-0.8 ± 0.03	22.7
GRB 110920A	0.8	-0.3 ± 0.03	-0.9 ± 0.04	2.0

Table 9
The evolution of the blackbody follows a broken power-law. However, the coarse time bins recovered by the Bayesian blocks algorithm make it difficult to constrain the decay indices.